# Rovibrational dynamics of the strontium molecule in the $A^1\Sigma_u^+$, $c^3\Pi_u$, and $a^3\Sigma_u^+$ manifold from state-of-the-art ab initio calculations

Wojciech Skomorowski
*Quantum Chemistry Laboratory, Department of Chemistry, University of Warsaw, Pasteura 1, 02-093 Warsaw, Poland*
Filip Pawłowski
*Physics Institute, Kazimierz Wielki University, pl. Weyssenhoffa 11, 85-072 Bydgoszcz, Poland and*
*Quantum Chemistry Laboratory, Department of Chemistry, University of Warsaw, Pasteura 1, 02-093 Warsaw, Poland*
Christiane P. Koch
*Theoretische Physik, Universität Kassel, Heinrich-Plett-Straße 40, 34132 Kassel, Germany*
Robert Moszynski
*Quantum Chemistry Laboratory, Department of Chemistry, University of Warsaw, Pasteura 1, 02–093 Warsaw, Poland*



State-of-the-art *ab initio* techniques have been applied to compute the potential energy curves for the electronic states in the $A^1\Sigma_u^+$, $c^3\Pi_u$, and $a^3\Sigma_u^+$ manifold of the strontium dimer, the spin-orbit and nonadiabatic coupling matrix elements between the states in the manifold, and the electric transition dipole moment from the ground $X^1\Sigma_g^+$ to the nonrelativistic and relativistic states in the A+c+a manifold. The potential energy curves and transition moments were obtained with the linear response (equation of motion) coupled cluster method limited to single, double, and linear triple excitations for the potentials and limited to single and double excitations for the transition moments. The spin-orbit and nonadiabatic coupling matrix elements were computed with the multireference configuration interaction method limited to single and double excitations. Our results for the nonrelativistic and relativistic (spin-orbit coupled) potentials deviate substantially from recent *ab initio* calculations. The potential energy curve for the spectroscopically active $(1)0_u^+$ state is in quantitative agreement with the empirical potential fitted to high-resolution Fourier transform spectra [A. Stein, H. Knöckel, and E. Tiemann, Eur. Phys. J. D **64**, 227 (2011)]. The computed *ab initio* points were fitted to physically sound analytical expressions, and used in converged coupled channel calculations of the rovibrational energy levels in the A+c+a manifold and line strengths for the $A^1\Sigma_u^+ \leftarrow X^1\Sigma_g^+$ transitions. Positions and lifetimes of quasi-bound Feshbach resonances lying above the $^1S_0 + {}^3P_1$ dissociation limit were also obtained. Our results reproduce (semi)quantitatively the experimental data observed thus far. Predictions for on-going and future experiments are also reported.

## I. INTRODUCTION

In recent years the strontium diatomic molecule, $Sr_2$, has attracted the interest of theoreticians and experimentalists. Similarly to the calcium dimer, $Sr_2$ in its ground $X^1\Sigma_g^+$ state does not form a chemical bond. Indeed, the binding energy of 1081.6 $cm^{-1}$[1] is typical for weakly bound complexes rather than for chemically bound molecules. However, excited states of $Sr_2$ are strongly bound, and have been observed in many experiments. As a matter of fact, the strontium molecule was the subject of numerous high-resolution spectroscopic studies in the gas phase[2,3] and in rare gas matrices[4,5]. The dissociation energy of the ground state was first estimated from the RKR inversion of the spectroscopic data for the $B^1\Sigma_u^+ \leftarrow X^1\Sigma_g^+$ transitions[3]. Recently, a more elaborate study of $Sr_2$ was reported[1], in which measurements of the $B^1\Sigma_u^+ \leftarrow X^1\Sigma_g^+$ transitions covering large parts of the ground state well were recorded. The spectrum corresponding to the $B^1\Sigma_u^+ \leftarrow X^1\Sigma_g^+$ transitions could easily be assigned using standard spectroscopic techniques because the B state dissociating into $^1S + {}^1P$ atoms is relatively well isolated, thus not perturbed by any other electronic state. While the same is true for the $A'^1\Pi_u$ state reported in Ref.[6], this is not the case for the $A^1\Sigma_u^+$ state dissociating into $^1S + {}^1D$ atoms. Here the potential energy curve of the A state crosses the curve of the $c^3\Pi_u$ state dissociating into $^1S + {}^3P$ states, and the corresponding spectrum cannot easily be assigned. Experimental investigation of the A state is limited to Ref.[6]. Tiemann and collaborators measured the spectrum corresponding to the $A^1\Sigma_u^+ \leftarrow X^1\Sigma_g^+$ transition by high-resolution Fourier transform spectroscopy, and showed that the rovibrational levels of the A state get strongly perturbed by the $c^3\Pi_u$ state[6]. Unfortunately, the amount of the measured data was not sufficient to apply a deperturbation procedure that could be used with trust to determine the spectroscopic constants of the $A^1\Sigma_u^+$ and $c^3\Pi_u$ states. In particular, the key information on the spin-orbit coupling between the A and c states could not be determined from the analysis of the spectra, and only an effective potential was obtained.

Most of the *ab initio* calculations on the $Sr_2$ molecule reported in the literature thus far are concerned with

the ground state potential energy curve[7,8] and the van der Waals constants governing the long-range behavior of the ground state potential[9–13]. To the best of our knowledge only three theoretical papers considered the excited states of the strontium dimer[14–16]. However, in view of the recent findings of Tiemann and collaborators[6] the quality of these data is questionable.

It should be stressed that alkaline-earth atoms and molecules are not only interesting for conventional spectroscopy, but are also intensely investigated in experiments at ultralow temperatures. Closed-shell atoms such as alkaline-earth metal atoms are much more challenging to cool and trap than open-shell atoms like the alkali atoms. They do not have magnetic moments in the ground state that would enable magnetic trapping. Moreover, the short lifetime of the first excited $^1P_1$ state implies rather high Doppler temperatures, requiring a dual-stage cooling with the second stage operating near the $^3P_1$ intercombination line. Despite these challenges, cooling of calcium, strontium, and ytterbium atoms to micro-Kelvin temperatures has been realized, and Bose-Einstein condensates of $^{40}Ca$[17], $^{84}Sr$[18,19], $^{86}Sr$[20], $^{88}Sr$[21], $^{170}Yb$[22], and $^{174}Yb$[23] have been obtained.

On the other hand, the closed-shell structure of the alkaline-earth metal atoms leads to very simple molecular potentials with low radiative losses and weak coupling to the environment. This opens new areas of possible applications, such as manipulation of the scattering properties with low-loss optical Feshbach resonances[24], high-resolution photoassociation spectroscopy at the intercombination line[25,26], precision measurements to test for a time variation of the proton-to-electron mass ratio[27,28] and of the fine structure constant[29], quantum computation with trapped polar molecules[30], and ultracold chemistry[31].

Of particular interest for the present work are the experimental investigations of the photoassociation spectra near the intercombination line[25,26,32] and proposed precision measurements of fundamental constants[27,28]. In particular the latter require a precise route for the production of ultracold molecules in predefined rovibrational states. This, in turn, requires an accurate knowledge of the potential energy curves and the various couplings that may occur in the $A^1\Sigma_u^+$, $c^3\Pi_u$, and $a^3\Sigma_u^+$ manifold of electronic states. Also, the assignment of the photoassociation spectrum requires a detailed knowledge of the rovibrational levels close to the dissociation limit. At present, the experimental data on the A state recorded to date[6] is far from complete. Therefore, in the present paper we report a theoretical study of the spectroscopy of the strontium dimer in the $A^1\Sigma_u^+$, $c^3\Pi_u$, and $a^3\Sigma_u^+$ manifold by state-of-the-art *ab initio* methods. The plan of this paper is as follows. In sec. II we describe the *ab initio* electronic structure and quantum dynamical calculations. We present the numerical results in sec. III and discuss at length the accuracy of the present results, compare with the available experimental data, and report predictions for the on-going experiments[33]. Finally, in sec. IV we conclude our paper.

## II. COMPUTATIONAL DETAILS

### A. Ab initio electronic structure calculations

In the present study we adopt the computational scheme successfully applied to the ground and excited states of the calcium dimer[34–38], magnesium dimer[39,40], $(BaRb)^+$ molecular ion[41], and SrYb heteronuclear molecule[42]. The potential energy curves for the lowest singlet and triplet excited ungerade states of the $Sr_2$ molecule corresponding to the $^1S + {}^3P$, $^1S + {}^3D$, and $^1S + {}^1D$ dissociation limits have been obtained by a supermolecule method:

$$V^{^{2S+1}|\Lambda|_u}(R) = E_{\rm AB}^{\rm SM} - E_{\rm A}^{\rm SM} - E_{\rm B}^{\rm SM}, \qquad (1)$$

where $E_{\rm AB}^{\rm SM}$ denotes the energy of the dimer computed using the supermolecule method (SM), and $E_{\rm X}^{\rm SM}$, X=A or B, is the energy of the atom X. Here, the molecular electronic term is denoted by $^{2S+1}|\Lambda|_u$ where $S$ is the total electronic spin quantum number, and $\Lambda$ the projection of the electronic orbital angular momentum on the molecular axis. The excited states were calculated employing the linear response theory (equation of motion) within the coupled-cluster singles, doubles, and linear triples (LRCC3) framework[43–45]. Note that in Refs.[34,35] the full configuration interaction correction (FCI) for the four-electron valence-valence correlation was added on top of the linear response result. However, the results for $Ca_2$[34,35] and more recently on $Mg_2$ show that for the states of interest this correction is so small that it can safely be neglected. We assume that this is also the case for $Sr_2$.

Transitions from the ground $X^1\Sigma_g^+$ state to the $^1\Sigma_u^+$ and $^1\Pi_u$ states are electric dipole allowed. The corresponding transition dipole moments are given by the following expression[46]:

$$\mu_i(n \leftarrow {\rm X}) = \langle {\rm X}^1\Sigma_g^+|r_i|(n)^1|\Lambda|_u\rangle, \qquad (2)$$

where $n$ numbers the consecutive nonrelativistic dissociation limits of the $^1|\Lambda|_u$ states, and $r_i$, $i = x, y$ or $z$, denotes the $i$th component of the position vector. Note that in Eq. (2), $i = x$ or $y$ corresponds to transitions to $^1\Pi_u$ states, while $i = z$ corresponds to transitions to $^1\Sigma_u^+$ states. In the present calculations the electric transition dipole moments were computed as the first residue of the coupled-cluster linear response function restricted to single and double excitations (LRCCSD) with two electric dipole operators[44]. Note that in principle the more advanced LRCC3 method could be used to calculate the transition moments. However, since the intensities in the spectra cannot be measured to a high precision, we have employed a less accurate method limited to single and double excitations. Comparison of the computed and measured atomic lifetimes will show below that such an

approximation is sufficient for the purpose of the present study.

The rovibrational energy levels of the electronically excited states of $Sr_2$ are expected to show some perturbations due to the nonadiabatic coupling between the electronic states. Analysis of the potential energy curves, cf. sec. III, reveals angular couplings of the $a^3\Sigma_u^+$ and $b^3\Sigma_u^+$ states with the $c^3\Pi_u$ state. Therefore, in this work we have computed the most important angular coupling matrix elements defined by the expression:

$$L(n \leftrightarrow n') = \langle (n)^{2S+1}|\Lambda|_u|L_\pm|(n')^{2S+1}|\Lambda'|_u\rangle, \qquad (3)$$

with $L_\pm$ the ladder operator of the electronic angular momentum and $n \leftrightarrow n'$ denoting the coupling between electronic states $n$ and $n'$ (here $n$ will stand for the $a^3\Sigma_u^+$ or $b^3\Sigma_u^+$ states, $n'$ for the $c^3\Pi_u$ state). Note that the electronic angular momentum operator couples states with the projection of the electronic orbital angular momentum on the molecular axis $\Lambda$ differing by one. In the present calculations the angular coupling between the triplet states was computed directly from the multireference configuration interaction wave functions limited to single and double excitations (MRCI).

Strontium is a heavy atom, and the electronic states of the $Sr_2$ molecule are expected to be strongly mixed by the spin-orbit interaction. Therefore, the spin-orbit coupling and its dependence on the internuclear distance $R$ must be taken into account in our analysis of the spectra in the mixed singlet/triplet $A^1\Sigma_u^+$, $c^3\Pi_u$, and $a^3\Sigma_u^+$ manifold of electronic states. We have evaluated the spin-orbit coupling matrix elements for the lowest dimer states that couple to the $0_u^+$ and $1_u$ states of $Sr_2$ within the MRCI framework. In our case the nonrelativistic states that are coupled through the spin-orbit interaction to the $0_u^+$ symmetry are $c^3\Pi_u$, $A^1\Sigma_u^+$ and $B^1\Sigma_u^+$[37,47]. Other electronic states of $Sr_2$ can be omitted from the present analysis due to their very weak couplings with the A+c+a manifold and significant energetic gaps as compared to these electronic states. Thus, the most important spin-orbit coupling matrix elements for states of the $0_u^+$ symmetry are given by

$$A(R) = \langle c^3\Pi_u(\Sigma = \pm 1, \Lambda = \mp 1)|\widehat{H}_{\rm SO}|c^3\Pi_u(\Sigma = \pm 1, \Lambda = \mp 1)\rangle\,, \qquad (4)$$

$$\xi_1(R) = \langle c^3\Pi_u(\Sigma = \pm 1, \Lambda = \mp 1)|\widehat{H}_{\rm SO}|A^1\Sigma_u^+\rangle\,, \qquad (5)$$

$$\xi_2(R) = \langle c^3\Pi_u(\Sigma = \pm 1, \Lambda = \mp 1)|\widehat{H}_{\rm SO}|B^1\Sigma_u^+\rangle\,, \qquad (6)$$

where $\widehat{H}_{\rm SO}$ is the spin-orbit Hamiltonian in the Breit-Pauli approximation[48] and $\Sigma$ denotes the projection of the electron spin angular momentum on the molecular axis. For the $1_u$ symmetry the most important couplings occur between the $c^3\Pi_u$, $a^3\Sigma_u^+$, $b^3\Sigma_u^+$ and $B'^1\Pi_u$ states[37,47], and the corresponding spin-orbit matrix elements read:

$$\varphi_1(R) = \langle c^3\Pi_u(\Sigma = 0, \Lambda = \pm 1)|\widehat{H}_{\rm SO}|a^3\Sigma_u^+(\Sigma = \pm 1, \Lambda = 0)\rangle\,, \qquad (7)$$

$$\varphi_2(R) = \langle c^3\Pi_u(\Sigma = 0, \Lambda = \pm 1)|\widehat{H}_{\rm SO}|b^3\Sigma_u^+(\Sigma = \pm 1, \Lambda = 0)\rangle\,, \qquad (8)$$

$$\varphi_3(R) = \langle c^3\Pi_u(\Sigma = 0, \Lambda = \pm 1)|\widehat{H}_{\rm SO}|B'^1\Pi_u\rangle\,, \qquad (9)$$

$$\zeta_1(R) = \langle a^3\Sigma_u^+(\Sigma = \pm 1, \Lambda = 0)|\widehat{H}_{\rm SO}|B'^1\Pi_u\rangle\,, \qquad (10)$$

$$\zeta_2(R) = \langle b^3\Sigma_u^+(\Sigma = \pm 1, \Lambda = 0)|\widehat{H}_{\rm SO}|B'^1\Pi_u\rangle\,. \qquad (11)$$

With the spin-orbit coupling matrix elements at hand, we can build up the matrices that will generate the potential energies of the spin-orbit states that couple to $0_u^+$ and $1_u$ symmetry. The matrices for the $0_u^+$ and $1_u$ states are given by:

$$\mathbb{V}^{0_u^+} = \begin{pmatrix} V^{c^3\Pi_u}(R) - A(R) & \xi_1(R) & \xi_2(R) \\ \xi_1(R) & V^{A^1\Sigma_u^+}(R) & 0 \\ \xi_2(R) & 0 & V^{B^1\Sigma_u^+}(R) \end{pmatrix} \qquad (12)$$

and

$$\mathbb{V}^{1_u} = \begin{pmatrix} V^{a^3\Sigma_u^+} & 0 & \varphi_1(R) & \zeta_1(R) \\ 0 & V^{b^3\Sigma_u^+} & \varphi_2(R) & \zeta_2(R) \\ \varphi_1(R) & \varphi_2(R) & V^{c^3\Pi_u}(R) & \varphi_3(R) \\ \zeta_1(R) & \zeta_2(R) & \varphi_3(R) & V^{B'^1\Pi_u}(R) \end{pmatrix}, \qquad (13)$$

respectively. Diagonalization of these matrices yields the spin-orbit coupled potential energy curves for the $0_u^+$ and $1_u$ states. Note that all the potentials in the matrices (12) and (13) are taken from the LRCC3 calculations. Only the diagonal and nondiagonal spin-orbit coupling matrix elements were obtained with the MRCI method. Once the eigenvectors of these matrices are available, one can easily get the electric dipole transition moments and the nonadiabatic coupling matrix elements between the relativistic states. It is worth noting that here, unlike in the case of $Ca_2$, the $B^1\Sigma_u^+$ and $B'^1\Pi_u$ states are included in the model. This is due to the fact that for $Sr_2$ the long-range spin-orbit interactions of the $c^3\Pi_u$ state with the B and B$'$ states have some significance since they are responsible for the existence of very weakly bound states located just below the $^1S_0 + {}^3P_1$ threshold that were observed in the photoassociation experiment by Zelevinsky *et al.*[26]. The long-range character of these couplings makes the photoassociation of the ultracold strontium atoms possible, yielding a non-negligible resonant $\delta C_3^{\rm res} R^{-3}$ interaction for the $0_u^+$ and $1_u$ potentials at the $^1S_0 + {}^3P_1$ asymptote, and a non-negligible relativistic transition moment from the $X^1\Sigma_g^+$ ground state. By contrast, the coupling with the $A'^1\Pi_u$ state which was reported in Ref.[6] was neglected in the present calculations

TABLE I. Parameters of the analytical fits of the $a^3\Sigma_u^+$, $b^3\Sigma_u^+$, $c^3\Pi_u$, and $A^1\Sigma_u^+$ potentials (in atomic units) for $Sr_2$. Numbers in parentheses denote the power of 10.

| Parameter | $a^3\Sigma_u^+$ | $b^3\Sigma_u^+$ | $c^3\Pi_u$ | $A^1\Sigma_u^+$ |
|---|---|---|---|---|
| $A_0$ | 6.763580846(2) | 3.812370308(5) | 5.806031460(6) | 1.0713571607(3) |
| $A_1$ | −2.7286531831(2) | −2.7785352110(5) | −3.433599894(6) | −3.1369577995(2) |
| $A_2$ | 4.4648343035(1) | 7.599745922(4) | 7.677597973(5) | 4.259633532(1) |
| $A_3$ | −3.4042105677 | −9.26259308(3) | −7.75564134(4) | −2.828788402 |
| $A_4$ | 0.1048331384 | 4.2607133921(2) | 3.0330564923(3) | 0.08207453705 |
| $\alpha$ | 0.03722198867 | 0.7652092533 | 2.102245892 | 0.2810137665 |
| $\beta$ | 3.14301181557 | 0.7516213273 | 1.03238202 | 1.195331858 |
| $\gamma$ | 0.07613828056 | 0.148486204 | 1.349678173(−3) | 0.0362537402 |
| $C_{12}$ | −5.318418476(9) | 1.1998965806(11) | −1.06415514(10) | 7.278665842(11) |
| $C_5$ | | | | −8.649(2) |
| $C_6$ | 4.488(3) | 6.750(3) | 3.951(3) | 2.72(3) |
| $C_8$ | 1.426(6) | 2.044(4) | 3.521(5) | 2.285(5) |
| $C_{10}$ | 2.321(8) | 1.010(6) | 3.296(7) | 9.223(7) |

since it is asymptotically zero for the $1_u$ states of interest and influences the $R^{-6}$ and higher asymptotics of the $(1)1_u$ state, as opposed to the $\delta C_3^{\rm res} R^{-3}$ asymptotics due to spin-orbit coupling with the $B'^1\Pi_u$ state, cf. Ref.[49] for a simple atomic model and Ref.[50] for a rigorous explanation. Note finally that the spin-orbit coupling between the $c^3\Pi_u$, $a^3\Sigma_u^+$, $b^3\Sigma_u^+$ and $B'^1\Pi_u$ states also leads to states of $0_u^-$ and $2_u$ symmetry. In the absence of strong nonadiabatic effects these states are not optically active and we do not discuss them here.

In order to mimic the scalar relativistic effects, some electrons were described by the ECP28MDF pseudopotential[51] from the Stuttgart library. Thus, in the present study the $Sr_2$ molecule was treated as a system of effectively 20 electrons. In all calculations the $[8s8p5d4f1g]$ basis set suggested in Ref.[51] was used, augmented by a set of $[1s1p1d1f3g]$ diffuse functions. In the calculations of the potentials this basis was supplemented by a set of *spdfg* bond functions[52]. The full basis of the dimer was employed in the supermolecule calculations and the Boys and Bernardi scheme was utilized to correct for the basis-set superposition error[53]. *Ab initio* calculations were performed for a set of 22 interatomic distances ranging from $R = 5$ to 50 bohr. In the calculations of the potential energy curves and transition dipole moments the DALTON code[54] was used. All MRCI calculations were done with the MOLPRO code[55]. We would like to emphasize that almost all *ab initio* results were obtained with the most advanced size-consistent methods of quantum chemistry, LRCC3 and LRCCSD. Only the spin-orbit coupling matrix elements and nonadiabatic matrix elements were obtained with the MRCI method which is not size consistent. Fortunately, all of the couplings are important in the region of the curve crossings or avoided crossings at short interatomic distances, so the effect of the size-inconsistency of MRCI on our results should not be dramatic.

### B. Analytical fits

The computed points of the potential energy curves were fitted to the following analytical expression:

$$V^{2S+1|\Lambda|_u}(R) = e^{-\alpha R-\gamma R^2}\sum_{i=0}^{4} A_i R^i + \frac{C_k^{\rm res}}{R^k} f_k(\beta, R) - \sum_{n=3}^{6} \frac{C_{2n}}{R^{2n}} f_{2n}(\beta, R), \qquad (14)$$

where $\{A_i\}_{i=0}^4$, $\alpha$, $\beta$, $\gamma$, and $C_{12}$ were adjusted to the computed points. The damping function $f_n(\beta, R)$ was employed in the form proposed by Tang and Toennies[56]. The long-range coefficients $\{C_{2n}\}_{n=3}^5$ were not fitted, but fixed at the *ab initio* values taken from Ref.[13]. In our case the leading long-range coefficient $C_k^{\rm res}$ describes the first-order resonant interaction[57] between the $Sr(^1S)$ and $Sr(^1D)$ atoms, and was also fixed at the *ab initio* value[13]. For the triplet states the resonant interaction term vanishes identically in the nonrelativistic approximation, so $C_k^{\rm res}$ is equal to zero. The parameters of the analytical fits of the potentials are reported in Table I.

The transition moments $\mu_0^{n\leftarrow X}(R)$, spin-orbit coupling matrix elements, $A(R)$, $\{\xi_i(R)\}_{i=1}^2$, $\{\zeta_i(R)\}_{i=1,2}$, $\{\varphi(R)\}_{i=1}^3$, and angular coupling matrix elements, $L(\mathrm{a}\leftrightarrow\mathrm{c})$ and $L(\mathrm{b}\leftrightarrow\mathrm{c})$, were fitted to the following generic expression:

$$X(R) = X^\infty + (A_0^X + A_1^X R + A_2^X R^2)e^{-\alpha_2^X R-\gamma^X R^2} + B^X e^{-\alpha_1^X R} + \sum_{n=n_0}^{6} \frac{X_n}{R^n} f_n(\beta^X, R), \qquad (15)$$

where $X$ stands for $\mu_0^{n\leftarrow X}(R)$, $A(R)$, $\{\xi_i(R)\}_{i=1}^2$, $\{\zeta_i(R)\}_{i=1}^2$, $\{\varphi(R)\}_{i=1}^3$, $L(\mathrm{a}\leftrightarrow\mathrm{c})$, and $L(\mathrm{b}\leftrightarrow\mathrm{c})$. The leading power in the inverse power expansion of Eq. (15) depends on the asymptotic multipole expansion of the wave functions in the polarization approximation[58–60]

and of the appropriate operator and varies between 3 and 6 for the different quantities $X$. The atomic values, $X^\infty$, were fixed as follows:

$$\begin{aligned} A^\infty &= \varphi_1^\infty = 193.68\ \mathrm{cm}^{-1}, \\ \varphi_3^\infty &= -\zeta_1^\infty = \xi_2^\infty/\sqrt{2} = -153.02\ \mathrm{cm}^{-1}, \end{aligned} \tag{16}$$

$$\xi_1^\infty = \varphi_2^\infty = \zeta_2^\infty = 0, \tag{17}$$

$$\mu_0^\infty(\mathrm{A} \leftarrow \mathrm{X}) = 0, \qquad \mu_0^\infty(\mathrm{B} \leftarrow \mathrm{X}) = \sqrt{2} \cdot 3.07\ \mathrm{a.u.}, \tag{18}$$

$$L^\infty(\mathrm{a} \leftrightarrow \mathrm{c}) = \sqrt{2}, \qquad L^\infty(\mathrm{b} \leftrightarrow \mathrm{c}) = 0, \tag{19}$$

and the remaining parameters were adjusted to the *ab initio* points. The value for $A^\infty$ was derived from the experimental positions of the states in the $^3$P multiplet assuming pure $LS$ coupling, while the values of $\xi_2^\infty$ and $\mu_0^\infty(\mathrm{B} \leftarrow \mathrm{X})$ are based on the present *ab initio* atomic calculations. The parameters of the analytical fits of the most important spin-orbit coupling matrix elements $A(R)$, $\xi_1(R)$, and $\xi_2(R)$ are reported in Table II. All parameters for other fitted quantities can be obtained from the authors upon request.

Note that fixing our fits at their proper asymptotic values is crucial for a proper description of the rovibrational transitions near the dissociation threshold. This is in a sharp contrast with some potentials fitted to the experimental data that may not be sufficiently sensitive to the long-range tail of the potential and spin-orbit couplings.

TABLE II. Parameters of the analytical fits of the spin-orbit coupling matrix elements (in atomic units) for $Sr_2$. Numbers in parentheses denote the power of 10.

| Parameter | $A(R)$ | $\xi_1(R)$ | $\xi_2(R)$ |
|---|---|---|---|
| $X^\infty$ | 8.824756(−4) | | −9.860287(−4) |
| $B^X$ | | 0.1281809 | −8.7008164(−3) |
| $\alpha_1^X$ | | 0.255215595 | 0.40876725 |
| $A_0^X$ | 0.254210634 | −8.18616724(−2) | 2.96378955(−6) |
| $A_1^X$ | −3.332647733(−2) | 9.17710750(−3) | −3.39493117(−7) |
| $A_2^X$ | | −4.77060945(−4) | 1.0586325(−8) |
| $\alpha_2^X$ | 0.7905806772 | | −0.92238515 |
| $\gamma^X$ | | 1.40267678(−2) | 2.8575636(−2) |
| $\beta^X$ | 1.3932739215 | 6.8008294 | 2.22429216 |
| $X_3$ | | | 2.64888569(−2) |
| $X_4$ | | −1.684296847 | |
| $X_6$ | −35.590169218 | | |

### C. Quantum-dynamical calculations

In the present paper we consider the homonuclear bosonic $^{88}Sr_2$ molecule. The rovibrational energy levels and wave functions for the ground $X^1\Sigma_g^+$ state were obtained by diagonalizing the Hamiltonian for the nuclear motion in the Born-Oppenheimer approximation with the variable step-size Fourier grid representation[61–63]. For the ground state, an accurate potential fitted to the experimental high-resolution Fourier transform spectra is available[1] and is used in our calculations.

Due to the spin-statistical weights for the bosonic $^{88}Sr_2$ molecule, we can limit ourselves to odd values of the rotational quantum number $J$ and $e$ parity levels[46]. Rovibrational energy levels for the excited electronic states in the $A^1\Sigma_u^+$, $c^3\Pi_u$, and $a^3\Sigma_u^+$ manifold were obtained by diagonalizing the following Hamiltonian:

$$\widehat{\mathbb{H}} = \begin{pmatrix} \widehat{H}_{\mathrm{diag}}^{\mathrm{c}^3\Pi_u} - A(R) & \xi_1 & \xi_2 & -C_{JL} & -C_{JL} & C_{JS} & 0 \\ \xi_1 & \widehat{H}_{\mathrm{diag}}^{\mathrm{A}^1\Sigma_u^+} & 0 & 0 & 0 & 0 & \sqrt{2}C_{JL} \\ \xi_2 & 0 & \widehat{H}_{\mathrm{diag}}^{\mathrm{B}^1\Sigma_u^+} & 0 & 0 & 0 & \sqrt{2}C_{JL} \\ -C_{JL} & 0 & 0 & \widehat{H}_{\mathrm{diag}}^{\mathrm{a}^3\Sigma_u^+} & 0 & \varphi_1 + C_{LS} & \zeta_1 \\ -C_{JL} & 0 & 0 & 0 & \widehat{H}_{\mathrm{diag}}^{\mathrm{b}^3\Sigma_u^+} & \varphi_2 + C_{LS} & \zeta_2 \\ C_{JS} & 0 & 0 & \varphi_1 + C_{LS} & \varphi_2 + C_{LS} & \widehat{H}_{\mathrm{diag}}^{\mathrm{c}^3\Pi_u} & \varphi_3 \\ 0 & \sqrt{2}C_{JL} & \sqrt{2}C_{JL} & \zeta_1 & \zeta_2 & \varphi_3 & \widehat{H}_{\mathrm{diag}}^{\mathrm{B}'^1\Pi_u} \end{pmatrix}, \tag{20}$$

where the diagonal term is given by:

$$\widehat{H}_{\mathrm{diag}}^{(n)^{(2S+1)}|\Lambda|_u} \equiv \frac{1}{2\mu}\widehat{p}_R^2 + V_n^{(2S+1)|\Lambda|_u}(R) + \frac{J(J+1) + S(S+1) + L(L+1) - \Omega^2 - \Sigma^2 - \Lambda^2}{2\mu R^2} \tag{21}$$

with $\widehat{p}_R$ denoting the radial momentum operator, $\mu$ the reduced mass of the dimer, and $\Omega$ is the projection of

the total electronic angular momentum on the molecular axis, so $\Omega = \Lambda + \Sigma$. The first three rows of the $\widehat{\mathbb{H}}$ matrix correspond to the states with $|\Omega| = 0$ while the last four rows to the states with $|\Omega| = 1$. The angular (Coriolis-type) couplings are defined as:

$$C_{JL}(R) = -\frac{[J(J+1)]^{1/2}\, L(R)}{2\mu R^2}, \tag{22}$$

$$C_{JS}(R) = -\frac{[2J(J+1)]^{1/2}}{2\mu R^2}, \tag{23}$$

$$C_{LS}(R) = 2^{1/2}\frac{L(R)}{2\mu R^2}, \tag{24}$$

where $L(R)$ stands for $L(n \leftrightarrow n')$ defined by Eq. (3) with $n$ and $n'$ properly chosen, the quantum number $L$ appearing in Eq. (21) is the electronic angular quantum number of the excited state atom, and all other symbols appearing in Eq. (20) are defined in Eqs. (4)–(6) and (7)–(11). We refer the reader to Ref.[37] for a rigorous justification of the above expressions. Note that the term $\frac{L(L+1)}{2\mu R^2}$ is not rigorously correct, since it results from the so-called adiabatic (diagonal) correction for the nuclear motion and the above mentioned value is true only in the separated atoms limit. At present, there is no *ab initio* electronic structure code that could provide us with (even approximate) values of the angular part of the adiabatic correction, so we keep it at its asymptotic atomic value. This approximation should work very well for the rovibrational levels near the dissociation threshold. If the nonadiabatic angular coupling matrix elements are small, we can set the Coriolis coupling constants $C_{JL}$, $C_{JS}$, and $C_{LS}$ equal to zero, and the matrix $\widehat{\mathbb{H}}$ becomes block diagonal with two blocks corresponding separately to the $0_u^+$ and $1_u$ levels:

$$\widehat{\mathbb{H}}^{0_u^+} = \begin{pmatrix} \widehat{H}^{\mathrm{c}^3\Pi_u}_{\mathrm{diag}} - A(R) & \xi_1 & \xi_2 \\ \xi_1 & \widehat{H}^{\mathrm{A}^1\Sigma_u^+}_{\mathrm{diag}} & 0 \\ \xi_2 & 0 & \widehat{H}^{\mathrm{B}^1\Sigma_u^+}_{\mathrm{diag}} \end{pmatrix}, \tag{25}$$

$$\widehat{\mathbb{H}}^{1_u} = \begin{pmatrix} \widehat{H}^{\mathrm{a}^3\Sigma_u^+}_{\mathrm{diag}} & 0 & \varphi_1 & \zeta_1 \\ 0 & \widehat{H}^{\mathrm{b}^3\Sigma_u^+}_{\mathrm{diag}} & \varphi_2 & \zeta_2 \\ \varphi_1 & \varphi_2 & \widehat{H}^{\mathrm{c}^3\Pi_u}_{\mathrm{diag}} & \varphi_3 \\ \zeta_1 & \zeta_2 & \varphi_3 & \widehat{H}^{\mathrm{B}'^1\Pi_u}_{\mathrm{diag}} \end{pmatrix}. \tag{26}$$

The line strength in the spectra, $S(v'J' \leftarrow v''J'')$, from the rovibrational level $|v'', J''\rangle$ of the ground electronic state to the rovibrational level $|v', J'\rangle$ of the $\mathrm{A}^1\Sigma_u^+$, $\mathrm{c}^3\Pi_u$, and $\mathrm{a}^3\Sigma_u^+$ manifold is given by:

$$S(v'J' \leftarrow v''J'') = (2J'+1)H_{J'} \times \Big| \sum_{\Omega'=0,\pm1} \sum_{\sigma=-1}^{1} \sum_{n'} \langle \chi_{1J''0}(v'') | r_\sigma(n' \leftarrow \mathrm{X}) | \chi_{n'J'\Omega'}(v') \rangle \Big|^2, \tag{27}$$

where $H_{J'}$ is the so-called Hönl-London factor,

$$H_{J'} = \begin{cases} \frac{J'+1}{2J'+1} & \text{for} \quad J' = J'' - 1, \\ \frac{1}{2J'+1} & \text{for} \quad J' = J'', \\ \frac{J'}{2J'+1} & \text{for} \quad J' = J'' + 1, \end{cases} \tag{28}$$

and $\chi_{1J''0}(v'')$ is the rovibrational wave function of the ground state, while $\chi_{n'J'\Omega'}(v')$ is an eigenfunction of the Hamiltonian, either $\widehat{\mathbb{H}}$ given by Eq. (20), or $\widehat{\mathbb{H}}^{0_u^+}$ and $\widehat{\mathbb{H}}^{1_u}$ given by Eqs. (25) and (26), if the helicity decoupling approximation (neglecting of the angular Coriolis couplings) is employed.

We also study the positions and lifetimes of Feshbach resonances appearing just above the $^1\mathrm{S}_0 + {}^3\mathrm{P}_1$ dissociation threshold. The Feshbach resonances of interest are quasi-bound rovibrational levels of the $(2)0_u^+$ electronic state lying above the dissociation limit of the $(1)0_u^+$ state, i.e., in the continuum of this state. Formally, the Feshbach resonances can be characterized by complex energies of the form $E_r - (i/2)\Gamma$, where $E_r$ denotes the position of the resonance state and $\Gamma$ its width which is directly related to the lifetime $\tau$ by $\tau = \hbar/\Gamma$. We have determined these complex energies by diagonalizing the Hamiltonian for the $0_u^+$ states, Eq. (25), with an imaginary absorbing potential $V_{\mathrm{CAP}}$ added to the diagonal Hamiltonian terms (21)[64–66]:

$$V_{\mathrm{CAP}}(R) = \begin{cases} 0 & , R \le R_{\mathrm{a}}, \\ \frac{4E_{\mathrm{min}}}{C^2}\left[\frac{1}{(1-x)^2} + \frac{1}{(1+x)^2} - 2\right] & , R_{\mathrm{a}} \le R < R_{\mathrm{max}}, \end{cases} \tag{29}$$

where $C = 2.62206$ and $x = (R - R_{\mathrm{a}})/(R_{\mathrm{max}} - R_{\mathrm{a}})$. The parameters $E_{\mathrm{min}}$, $R_{\mathrm{a}}$, and $R_{\mathrm{max}}$ were adjusted to obtain stable results with respect to small variations of these parameters. Approximate positions of the resonances were first determined by using the stabilization method[67] with respect to the size of the grid. With these positions at hand, a set of parameters leading to stable complex eigenvalues corresponding to the positions and widths of the resonances was easily found, yielding $R_{\mathrm{a}} = 30$ bohr, $R_{\mathrm{max}} = 200$ bohr, and $E_{\mathrm{min}} = 30$ cm$^{-1}$. The knowledge of the approximate positions was particularly useful to determine the value of $E_{\mathrm{min}}$.

## III. NUMERICAL RESULTS AND DISCUSSION

### A. Ab initio electronic structure data

Before discussing the potential energy curves, we first discuss the atomic excitation energies obtained from the LRCC3 calculations and the atomic lifetimes. In Table III we present calculated excitation energies in comparison with fully relativistic atomic calculations of Porsev and collaborators[68] and experimental data. Our predicted position of the nonrelativistic $^3$P state is 14570.8 cm$^{-1}$, to be compared with the experimental value of 14704.9 cm$^{-1}$[69] deduced from the positions of the states

TABLE III. Excitation energies (in $cm^{-1}$) for the low-lying energy levels of strontium atom.

| Excited state | Present | Reference[68] | Experiment[69] |
|---|---|---|---|
| $^3P_0$ | 14187.3 | 14241 | 14317.5 |
| $^3P_1$ | 14372.7 | 14448 | 14504.4 |
| $^3P_2$ | 14762.6 | 14825 | 14898.6 |
| $^3D_1$ | 18582.9 | 18076 | 18159.1 |
| $^3D_2$ | 18637.2 | 18141 | 18218.8 |
| $^3D_3$ | 18726.0 | 18254 | 18319.3 |
| $^1D_2$ | 20650.3 | 19968 | 20149.7 |
| $^1P_1$ | 21764.3 | 21469 | 21698.5 |

in the $^3P$ multiplet and the Landé rule. For the $^1P_1$ state we obtain 21764.3 $cm^{-1}$, again in very good agreement with the experimental value of 21698.5 $cm^{-1}$[69]. For the nonrelativistic $^3D$ state we obtain 18668.8 $cm^{-1}$, to be compared with 18255.2 $cm^{-1}$[69] deduced from the positions of the states in the $^3D$ multiplet and the Landé rule. Finally, our term energy for the $^1D_2$ state is 20650.3 $cm^{-1}$, again in a satisfactory agreement with experiment, 20149.7 $cm^{-1}$[69]. The accuracy of the atomic spin-orbit couplings can be judged by comparing the computed and observed splittings of the energy levels in the $^3P$ and $^3D$ multiplets. For the $^3P$ multiplet, theoretical splittings between the $^3P_2$ and $^3P_1$, $^3P_2$ and $^3P_0$, and $^3P_1$ and $^3P_0$ levels amount to 389.9 $cm^{-1}$, 575.3 $cm^{-1}$, and 185.4 $cm^{-1}$, respectively, to be compared with the experimental numbers, 394.2 $cm^{-1}$, 581.0 $cm^{-1}$, and 186.8 $cm^{-1}$, respectively. A somewhat less good agreement is observed for the $^3D$ multiplet. The theoretical fine splittings for the $^3D_3$–$^3D_2$, $^3D_3$–$^3D_1$, and $^3D_2$–$^3D_1$ states read 88.9 $cm^{-1}$, 143.1 $cm^{-1}$, and 54.2 $cm^{-1}$, respectively, while the experimental numbers are 100.5 $cm^{-1}$, 160.2 $cm^{-1}$, and 59.7 $cm^{-1}$, respectively. Finally, we also note that the lifetimes of the $^3P_1$, multiplet $^3D$, $^1D_2$, and $^1P_1$ states of Sr are accurately reproduced. Our calculated lifetimes together with the most recent experimental and other theoretical results are listed in Table IV. For the $^1P_1$ state we obtained 5.09 ns to be compared with the experimental value of 5.22(3) ns[70]. For $^3P_1$ the theoretical and experimental numbers are 21.4 $\mu$s and 21.5(2) $\mu$s[26], respectively. For the D states we observe a slightly worse agreement. The theoretical lifetime of the $^1D_2$ state is 0.23 ms, to be compared with the experimental value of 0.30 ms[71]. The same numbers for the average multiplet $^3D$ are 2.72 $\mu$s and 2.5(2) $\mu$s[72]. Such a good agreement between theory and experiment for the atoms gives us confidence that the molecular results will be of similar accuracy, i.e., at worst a few percent off from the exact results.

One of the important issues in *ab initio* electronic structure calculations is the quality of the basis set and of the wave functions. To further judge the quality of the basis set used in our calculations we have computed the leading $C_6$ van der Waals coefficient for the ground $X^1\Sigma_g^+$ state. This coefficient was obtained by using the explicitly connected representation of the expectation value and polarization propagator within the coupled cluster method[73,74], and the best approximation XCCSD4 proposed by Korona and collaborators[75]. Our *ab initio* result is 3142 a.u. which compares very favorably with the value fitted to high-resolution Fourier transform spectra, 3168(10) a.u.[1]. The agreement between theory and experiment is better than for most of the other *ab initio* calculations[9–13]. Comparison between theory and experiment for the well depth of the ground state $X^1\Sigma_g^+$ potential is somewhat less satisfactory. Our theoretical value is 1124.0 $cm^{-1}$, to be compared with the experimental result of 1081.64(2) $cm^{-1}$[1], i.e., 3.8% too large. However, in the case of the ground state interaction, the FCI correction for the valence-valence correlation turned out to be important. Due to computational limitations, we could obtain it only in the Sadlej pVTZ basis[76] which is comparatively small and does not allow for a better accuracy.

TABLE IV. Comparison of the present and most recent theoretical and experimental values of the lifetimes of low-lying excited states of strontium atom.

| Excited state | lifetime | Reference |
|---|---|---|
| $^1P_1$ | 5.09 ns | Present |
| | 5.38 ns | Theory, Ref.[68] |
| | 5.35 ns | Theory, Ref.[13] |
| | 5.22(3) ns | Experiment, Ref.[70] |
| | 5.263(4) ns | Experiment, Ref.[79] |
| $^3P_1$ | 21.40 $\mu$s | Present |
| | 24.4 $\mu$s | Theory, Ref.[80] |
| | 19.0 $\mu$s | Theory, Ref.[81] |
| | 21.5(2) $\mu$s | Experiment, Ref.[26] |
| $^1D_2$ | 0.23 ms | Present |
| | 0.412(10) ms | Experiment, Ref.[82] |
| | 0.30 ms | Experiment, Ref.[71] |
| $\overline{^3D}$ | 2.72 $\mu$s | Present |
| | 2.4 $\mu$s | Theory, Ref.[68] |
| | 2.5(2) $\mu$s | Experiment, Ref.[72] |

The nonrelativistic potential energy curves relevant for the spectroscopy in the A+c+a manifold are plotted in Fig. 1, while the spectroscopic characteristics of these states are reported in Table V. The separated atoms energy for each state was set equal to the experimental value. Due to the computational limitations in the present work we did not consider the $B^1\Sigma_u^+$, $A'^1\Pi_u$ and $B'^1\Pi_u$ states. Fortunately enough, the calculations of these potentials were not crucial for our study. Indeed, the potential energy curve for the $B^1\Sigma_u^+$ state, with the correct $C_3^{\rm res}R^{-3}$ asymptotics, could be fitted to the experimental data, and is available in the literature[6]. According to Ref.[6], the $A'^1\Pi_u$ state is isolated, and its rovibrational levels are only weakly perturbed. Thus, it can safely be omitted from our model for the rovibrational levels of the $1_u$ states near the $^1S_0 + {}^3P_1$ thresh-

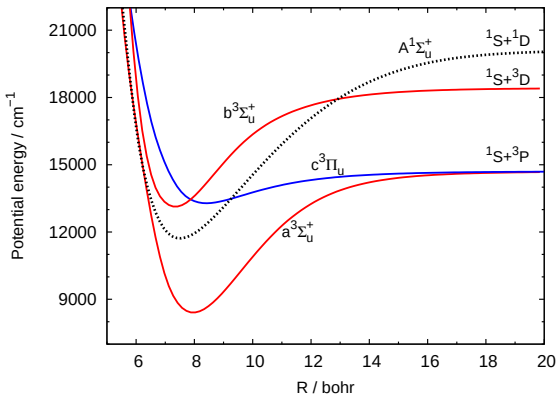


FIG. 1. *Ab initio* potential energy curves for the $A^1\Sigma_u^+$, $c^3\Pi_u$, $a^3\Sigma_u^+$, and $b^3\Sigma_u^+$ states of the strontium dimer.

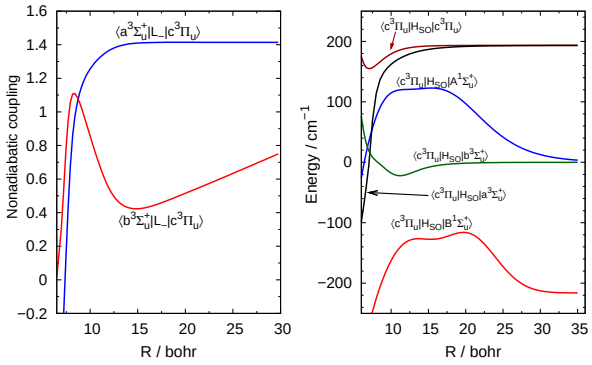


FIG. 2. Nonadiabatic matrix elements (left-hand panel) and spin-orbit coupling matrix elements (right-hand panel) as functions of the interatomic distance $R$.

old. However, would this state become interesting from an experimental point of view, an accurate potential energy curve fitted to the observed spectroscopic transitions is available in Ref.[6], while the important spin-orbit coupling matrix elements can be obtained from the present authors upon request. The second state dissociating into the $^1S + ^1P$ atoms, the $B'^1\Pi_u$ state, was not observed experimentally. In our work the potential energy curve for this state was approximated with its long-range form $C_3^{\rm res}R^{-3}$, with the proper long-range coefficient adapted from Ref.[13]. While this is an approximation, it is not a crucial one, since the spin-orbit coupling of this state with the $c^3\Pi_u$ state is important only at large interatomic distances, where it becomes constant, and affects the rovibrational dynamics of the $Sr_2$ molecule only near the intercombination line $^1S_0 + ^3P_1$.

Let us compare our results with other available *ab initio* data from nonrelativistic calculations[15]. The spectroscopic constants are listed in Table V and compared to the results of Ref.[15]. Inspection of Table V shows that

TABLE V. Spectroscopic characteristics of the nonrelativistic electronic states of $Sr_2$ dimer.

| State | $D_e$/cm$^{-1}$ | $R_e$/bohr | Ref. | Dissociation |
|---|---|---|---|---|
| $a^3\Sigma_u^+$ | 6298 | 7.95 | Present | $^1S+^3P$ |
| | 6895 | 7.74 | [15] | |
| | 6683 | 7.79 | [14] | |
| $b^3\Sigma_u^+$ | 5293 | 7.33 | Present | $^1S+^3D$ |
| | 4698 | 7.25 | [15] | |
| | 5763 | 7.08 | [14] | |
| $c^3\Pi_u$ | 1422 | 8.41 | Present | $^1S+^3P$ |
| | 1892 | 8.02 | [15] | |
| | 1785 | 8.16 | [14] | |
| $A^1\Sigma_u^+$ | 8433 | 7.54 | Present | $^1S+^1D$ |
| | 5440 | 7.12 | [15] | |
| | 9066 | 7.28 | [14] | |

the agreement with the data of Czuchaj *et al.*[15] is not satisfactory. For most of the states the computed electronic binding energies agree within a few hundred cm$^{-1}$ at best, while the differences in the positions of the minima are 0.4 bohr at worst. The most striking difference between the present results and the data of Ref.[15] is the spectroscopically active $A^1\Sigma_u^+$ state. Here, the difference in the position of the minimum is 0.42 bohr, and the difference in $D_e$ is as much as 4000 cm$^{-1}$. Surprisingly, the agreement of the present results with the older 1996 calculations by Aubert-Frécon and collaborators[14] is comparatively good. Except for the $c^3\Pi_u$ state, the well depths agree within 6% to 8% and the well positions within 0.3 bohr at worst. For the $c^3\Pi_u$ state we note a serious disagreement to all previous results. Our potential is considerably shallower and the minimum is shifted to larger distances. However, as will be shown in sec. III B the present picture of the interatomic interactions in the A+c+a manifold reproduces all features of the available experimental data.

The nonadiabatic and spin-orbit coupling matrix elements as functions of the interatomic distance $R$ are reported in Fig. 2. Note the maximum in the angular coupling between the $c^3\Pi_u$ and the $b^3\Sigma_u^+$ states. The position of this maximum corresponds to the crossing of the potential energy curves of these states. Also worth noting is the broad maximum of the spin-orbit coupling between the $A^1\Sigma_u^+$ and $c^3\Pi_u$ states. This maximum extends to the region where the potential energy curves cross, and is responsible for the strong mixing of the singlet and triplet rovibrational energy levels. At large distances this particular coupling tends to zero, but the coupling between the $B^1\Sigma_u^+$ and the $c^3\Pi_u$ states becomes important and is responsible for the nonvanishing relativistic dipole moment between the ground state and the triplet levels in the A+a+c manifold.

The relativistic $0_u^+$ and $1_u$ potentials as functions of the interatomic distance $R$ are depicted in Fig. 3. Their spectroscopic parameters are reported in Table VI. First, we note an excellent agreement between the present *ab initio*

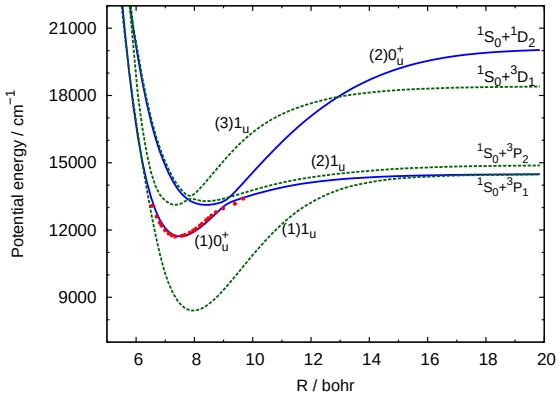


FIG. 3. Relativistic potential energy curves for the lowest $0_u^+$ and $1_u$ states of the strontium dimer. The dots represent the effective empirical potential fitted to the high-resolution Fourier transform spectroscopic data of Ref.[6].

potential for the $(1)0_u^+$ state and the effective empirical potential fitted to the high-resolution Fourier transform spectroscopic data[6]. The well depths, 2782 cm$^{-1}$ on the theory side and 2790 cm$^{-1}$ from the fit to the experimental data, agree within 8 cm$^{-1}$, while the well positions agree to within 0.05 bohr. It is gratifying to observe that the present *ab initio* calculations also reproduce satisfactorily the position and energy of the avoided crossing. Theory predicts the avoided crossing between the (1) and $(2)0_u^+$ potentials at $R$ = 9.1 bohr and $V$ = –1357 cm$^{-1}$, while the experimental numbers are $R$ = 9.1 bohr and $V$ = –1470 cm$^{-1}$. We note a substantial disagreement between the present *ab initio* results and those reported by Kotochigova[16]. The difference in the well depth is as large as 946 cm$^{-1}$. This means that Ref.[16] does not predict any interaction between the (1) and $(2)0_u^+$ states. Thus, our result fully confirms the disagreement already noticed by Tiemann and collaborators[6]. For other states

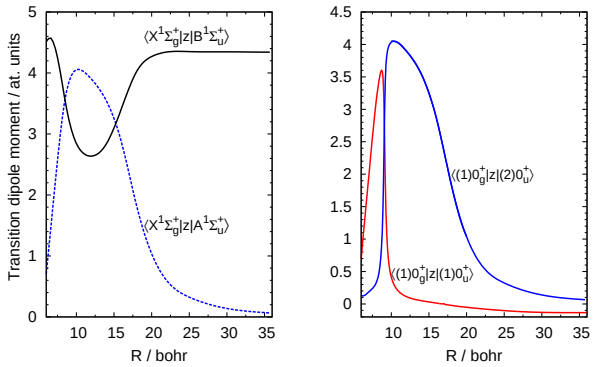


FIG. 4. Transition dipole moments between the ground electronic state and the excited states of $Sr_2$ in the non-relativistic basis (left-hand panel) and the relativistic basis (right-hand panel) as functions of the interatomic distance $R$.

TABLE VI. Spectroscopic characteristics of the relativistic electronic states of $Sr_2$ dimer.

| State | $D_e$/cm$^{-1}$ | $R_e$/bohr | Ref. | Dissociation |
|---|---|---|---|---|
| $(1)0_u^+$ | 2782 | 7.51 | Present | $^1$S$_0$+$^3$P$_1$ |
| | 2790 | 7.46 | [6] | |
| | 1837 | 8.2 | [16] | |
| $(2)0_u^+$ | 7039 | 8.39 | Present | $^1$S$_0$+$^1$D$_2$ |
| | 5292 | 7.2 | [16] | |
| $(1)1_u$ | 6097 | 7.95 | Present | $^1$S$_0$+$^3$P$_1$ |
| | 6921 | 7.8 | [16] | |
| $(2)1_u$ | 1942 | 7.34 | Present | $^1$S$_0$+$^3$P$_2$ |
| | 1907 | 8.2 | [16] | |
| $(3)1_u$ | 4863 | 7.97 | Present | $^1$S$_0$+$^3$D$_1$ |
| | 4849 | 7.4 | [16] | |

the agreement between the two calculations is quite erratic. For instance, the well depths for the second state of $0_u^+$ symmetry and the first state of $1_u$ symmetry differ substantially, while the results for the $(2)1_u$ and $(3)1_u$ states are very close in energy, but the positions of the wells are shifted by as much as 0.5 to 0.9 bohr.

Fig. 4 shows the nonrelativistic electric transition dipole moments from the ground state to the $^1\Sigma_u^+$ states and the relativistic transition dipole moments to the $0_u^+$ states. Inspection of Fig. 4 reveals a broad maximum in the transition moment to the $A^1\Sigma_u^+$ state at distances around the minimum of the ground $X^1\Sigma_g^+$ state, and decay to zero at large distances. The transition moment to the $B^1\Sigma_u^+$ state exhibits a broad minimum in the very same region and tends to the atomic value at large distances. The two relativistic curves reported in the right-hand panel of Fig. 4, when superimposed, reproduce the transition moment to the $A^1\Sigma_u^+$ state. This is not surprising, since at small distances the relativistic transition moment to the $(1)0_u^+$ is dominated by the singlet component. Around the crossing between the $A^1\Sigma_u^+$ and the $c^3\Pi_u$ it drops off drastically due to the predominantly triplet character of the electronic wave function. Note that at large distances it does not decay to zero, but rather to a small but constant atomic value reflecting the finite lifetime of the atomic $^3P_1$ state. The opposite picture holds for the transition moment to the $(2)0_u^+$ state. At small distances this state is dominated by the triplet component, and the transition moment is very small. Starting from the curve crossing, the $(2)0_u^+$ state is predominantly singlet, and the transition dipole moment becomes very large.

### B. Energy levels and rovibrational spectra of $Sr_2$ in the $A^1\Sigma_u^+$, $c^3\Pi_u$, and $a^3\Sigma_u^+$ manifold

Before comparing our results with the existing experimental data, let us discuss the validity of the decoupling between the $0_u^+$ and $1_u$ states. Similarly as for the

$Ca_2$[37] and SrYb[42] molecules, the nonadiabatic angular coupling is completely negligible also for the strontium dimer, except for a few most weakly bound levels. We have calculated the bound states for all possible values of the rotational quantum number $J$ by diagonalization of the full Hamiltonian matrix (20) with the variable step Fourier grid representation, and submatrices corresponding to the $0_u^+$ and $1_u$ blocks, Eqs. (25) and (26). We found that the eigenvalues of the decoupled matrices differ from the eigenvalues of the full matrix by less than $10^{-3}$ cm$^{-1}$, justifying the decoupled representation. Actually, experimental data for the rovibrational energy levels of the $(1)1_u$ state are scarce and limited to three levels closest to the $^1S_0 + {}^3P_1$ dissociation limit, so we will focus our discussion on the $0_u^+$ levels.

We have generated all energy levels for the $0_u^+$ and $1_u$ states up to and including $J' = 219$. Comparison of the computed energy levels for the $0_u^+$ state with the data derived from the high-resolution Fourier transform spectroscopy show a root-mean-square-deviation (RMSD) between theory and experiment of 10.5 cm$^{-1}$. While such an agreement between theory and experiment is very good for a system with 76 electrons, we decided to adjust the *ab initio* data to the existing experimental data to lower the RMSD. This allows us to make reliable predictions for the ongoing experiments on ultracold strontium molecules[33]. It turned out that by slightly changing the $A_0$ and $C_{12}$ parameters by 0.03% and 0.19%, respectively, in the analytical expression for the $A^1\Sigma_u^+$ potential, Eq. (14), we could reduce the RMSD for $J' = 1$ to 0.64 cm$^{-1}$. With the new values of the $A_0$ and $C_{12}$ parameters, the root-mean-square-deviation of our results for $J' \leq 50$, as compared to the raw data of Tiemann and collaborators (see the supplementary material of Ref.[6]) is 4.5 cm$^{-1}$. We must admit, however, that the present fit is not perfect for very high values of $J'$. Fortunately, these values of the rotational quantum number $J'$ are not of interest

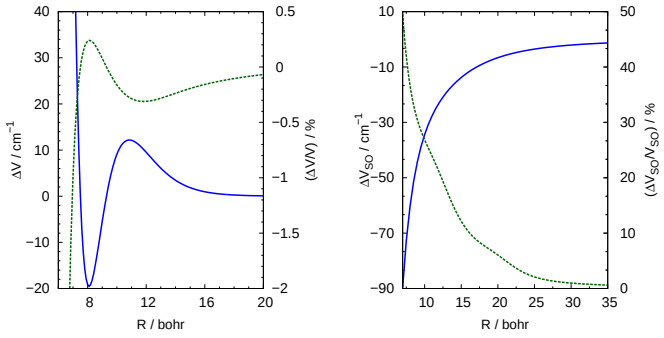


FIG. 5. Left-hand panel: Comparison of the original $A^1\Sigma_u^+$ potential with the fitted one to the experimental data[6] for $J' = 1$. The solid blue line shows the absolute difference, $\Delta V = V_{\text{fitted}}$-$V_{ab\ initio}$, while the green dashed line shows the relative difference, $\frac{\Delta V}{V} = \frac{V_{\text{fitted}} - V_{ab\ initio}}{V_{ab\ initio}} \cdot 100\%$. Right-hand panel: the same for the spin-orbit coupling term $\xi_2 = \langle c^3\Pi_u | H_{SO} | B^1\Sigma_u^+ \rangle$.

for the ultracold experiments such as photoassociation spectroscopy[26] or precision measurements leading to the determination of the time variation of the electron to proton mass ratio[27,28]. To better reproduce the levels near the $^1S_0 + {}^3P_1$ threshold[26], we have adjusted the spin-orbit coupling between the $c^3\Pi_u$ and $B^1\Sigma_u^+$ states, Eq. (6). Specifically, we varied the parameters $X^\infty$, $B^X$, and $X_3$ in the fit of $\xi_2(R)$. The adjustments introduced to our *ab initio* data are illustrated in Fig. 5. Quantitatively, the adjusted and *ab initio* potentials for the $A^1\Sigma_u^+$ state differ by 290 cm$^{-1}$ in the repulsive region, at $R = 6.5$ bohr, by -2.6 cm$^{-1}$ at the minimum, $R = 7.54$ bohr, and by 0.07 cm$^{-1}$ in the long range, at $R = 20$ bohr. All these differences represent at most 2.5% of the original *ab initio* potential. Such an accuracy of the *ab initio* calculations for a system of this size would be purely accidental. For the spin-orbit term $\xi_2(R)$, the adjustment results in a change by nearly 50% in the repulsive region and less than 0.3% in the asymptotic value. Here, the shifts were relatively more important than in the case of the $A^1\Sigma_u^+$ potential, and this can be attributed to the lower accuracy of the results from the MRCI method, which was employed for the calculation of the spin-orbit coupling. It should be stressed, however, that only the long-range value of the $\xi_2(R)$ coupling has some significance for the described dynamics of the $Sr_2$ molecule, as it affects positions of the most weakly bound levels below the $^1S_0 + {}^3P_1$ threshold. Note that the parameters reported in Tables I and II are those adjusted to the experimental data for $J' = 1$.

From Figs. 1 and 3 we expect that some of the rovibrational levels can be assigned to a single state, $A^1\Sigma_u^+$ or $c^3\Pi_u$, while some of them will show a strongly mixed singlet/triplet character. This is indeed the case, as is nicely illustrated by Fig. 6. The contour plots of the $A^1\Sigma_u^+$ and $c^3\Pi_u$ state populations clearly show that for lower values of $J'$ all levels with $v' \leq 18$ are predominantly singlet levels of the $A^1\Sigma_u^+$ state. By contrast, the $v' = 19$ level is the first level that can fully be assigned to the $c^3\Pi_u$ state. This is also clear by comparing the energies of this particular level in the coupled model and in the Born-Oppenheimer approximation: 1363 cm$^{-1}$ vs. 1398 cm$^{-1}$. At higher values of $v'$ the situation becomes quite erratic and most of the levels are of strongly mixed singlet/triplet character. Only at high values of $v'$ the levels can again be assigned, this time to the $c^3\Pi_u$ state, although some regions of strong mixing are observed, e.g., near $v' = 84$ or $v' = 95$. Such a mixing in the rovibrational levels close to the dissociation limit is very important for the ongoing photoassociation experiments of ultracold strontium atoms and is discussed in detail in Ref.[77].

More detailed information on the strongly mixed levels is obtained by examing the rotational constants $B_{v'}$ as function of the binding energy of the rovibrational level $|v', J'\rangle$. This is illustrated in the left-hand panel of Fig. 7, showing the first 19 levels from $v' = 0$ to 18 not to be perturbed, with a uniform nearly linear dependence of

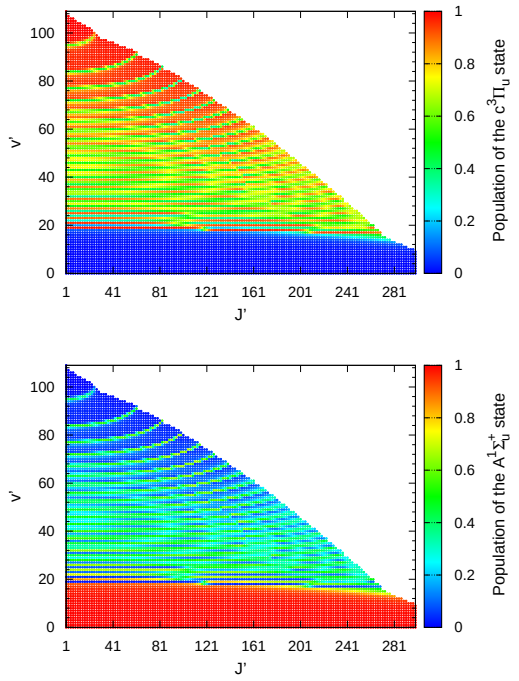


FIG. 6. Population of the $c^3\Pi_u$ and $A^1\Sigma_u^+$ components of the $0_u^+$ rovibrational levels lying below the $^1S_0 + {}^3P_1$ asymptote.

the rotational constant on the binding energy. Starting from $v' = 18$ the linear dependence is clearly broken, and the curve is characterized by irregular behaviour. However, it is still possible to distinguish levels which are almost purely triplet. The rotational spacings as functions of $J'(J'+1)$ reported in the right-hand panel of Fig. 7 give information about the perturbed levels. Indeed, the rotational spacing for $v' = 0$ shows a purely linear character as a function of $J'(J'+1)$. For $v' = 16$ this linear dependence is broken for high values of $J'$, but the nonlinear character is due to the centrifugal distortion, and not to the triplet perturbations only. Starting from

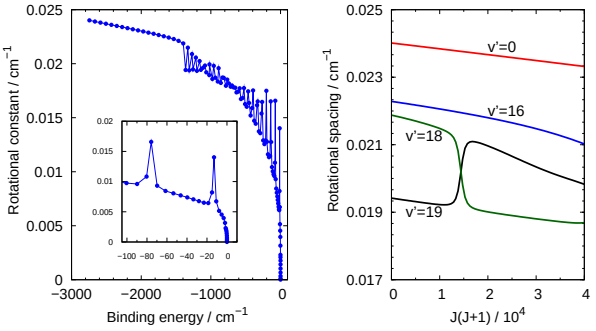


FIG. 7. Rotational constant of the $0_u^+$ rovibrational levels for $J = 1'$ (left-hand panel) and rotational spacing, defined by $\Delta E_{vJ}/(4J-2)$ (right-hand panel).

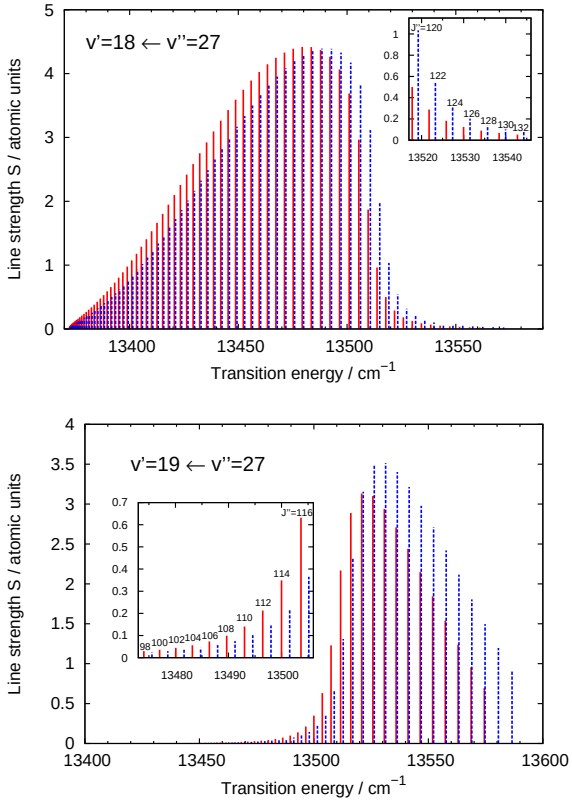


FIG. 8. Line strengths corresponding to the $P$ (red solid) and $R$ (blue dashed) branches in the band $\nu' = 18 \leftarrow \nu'' = 27$ (upper panel) and $\nu' = 19 \leftarrow \nu'' = 27$ (lower panel). The spectral lines in the figures are labeled by the rotational quantum number $J''$ of the initial state.

$v' = 18$, the rovibrational levels can have very different character (purely triplet or singlet, strongly mixed), depending on the value of $J'$. This is clearly illustrated by the sudden changes in the slope of the linear dependence of the rotational spacing on $J'(J'+1)$.

Figure 8 reports the line strengths for the transitions $v' = 18 \leftarrow v'' = 27$ and $v' = 19 \leftarrow v'' = 27$ for different values of the rotational quantum number $J''$ of the initial state. The level $v'' = 27$ was chosen since it plays a central role in proposed experiments to determine a time variation of the electron to proton mass ratio[27,28]. Inspection of Fig. 8 reveals that the spectral line strengths for the $v' = 18 \leftarrow v'' = 27$ transitions show a typical dependence on the transition frequency, with a slow increase as a function of $J''$, and a relatively steep and fast decrease for large transition frequencies. By contrast, the line strengths for the $v' = 19 \leftarrow v'' = 27$ transitions show a completely different dependence on the transition frequency. First we observe a very slow increase of the line strength with the increasing $J''$, see the insert and note the difference in the intensity scale, and a very slow decrease at large values of the transition frequency. Such a behaviour is again a signature of strong perturbations

from the $c^3\Pi_u$ state that should be observable in experiment.

### C. Feshbach resonances above the $^1S_0 + ^3P_1$ asymptote

The rovibrational states that could be assigned to the $(2)0_u^+$ state lying above the $^1S_0 + ^3P_1$ dissociation limit are embedded in the continuum of the $(1)0_u^+$ state, and thus are Feshbach resonances, i.e., quasi-bound states with finite lifetimes. Two decay mechanisms are possible depending on the strength of the coupling with the continuum. The resonances can decay to the $^1S_0 + ^3P_1$ continuum, i.e., dissociate into atoms (predissociation), or, if the lifetime is long enough, decay to bound or continuum states of the electronic ground state (spontaneous emission). Our computed positions, widths, and lifetimes of a few low lying Feshbach resonances for $J' = 1$ are reported in Table VII. The width of the resonances varies quite strongly, between almost 1 $cm^{-1}$ for the very broad one to $\approx$0.001 $cm^{-1}$ for the very narrow one. The corresponding lifetimes also vary considerably, from the picosecond to the nanosecond scale. This implies that some of the resonances should be observable in high-resolution Fourier transform spectroscopic experiments.

In Table VII we have numbered the resonant states by the vibrational quantum number $v'$ corresponding to bound vibrational states above the $^1S_0 + ^3P_1$ dissociation limit that result from the diagonalization of the $\widehat{\mathbb{H}}^{0_u^+}$ Hamiltonian. For $J' = 1$ we have found 110 bound levels of the $0_u^+$ symmetry which lie below the $^1S_0 + ^3P_1$ asymptote, assigning them vibrational quantum numbers ranging $v' = 0$ to $v' = 109$. Thus the first quasi-bound level reported in Table VII located above the $^1S_0 + ^3P_1$ threshold has the vibrational quantum number $v' = 110$. Only eigenvalues that were stable with respect to the grid size were selected, and the exact positions and lifetimes were determined with the complex absorbing potential of Eq. (29). It turns out that the width/lifetime is a very sensitive function of the strength of the spin-orbit coupling. To illustrate this point, we report the widths of the resonant states as a function of the triplet state population of the rovibrational wave function in the left-hand panel of Fig. 9. The narrow resonances are found

TABLE VII. Positions (relative to the $^1S_0 + ^3P_1$ threshold), widths, and lifetimes of the Feshbach resonances of $^{88}Sr_2$ above the $^1S_0 + ^3P_1$ dissociation limit.

| $v'$ | $E_r/cm^{-1}$ | $\Gamma/cm^{-1}$ | $\tau$/ns |
|---|---|---|---|
| 110 | 49.8 | 0.8761 | 0.0037 |
| 111 | 112.2 | 0.4658 | 0.0067 |
| 112 | 174.4 | 0.1924 | 0.0162 |
| 113 | 236.3 | 0.0410 | 0.0759 |
| 114 | 297.9 | 0.0008 | 3.8821 |
| 115 | 359.2 | 0.0638 | 0.0488 |

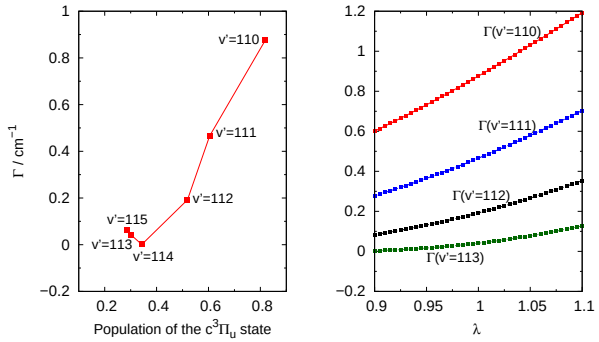


FIG. 9. Widths of the Feshbach resonances as a function of the population of the $c^3\Pi_u$ state and scaling parameter $\lambda$ of the spin-orbit term $\langle c^3\Pi_u|H_{SO}|A^1\Sigma_u^+\rangle$.

to be dominated by the singlet component of the wave function, for which the coupling through the spin-orbit interaction is weak. By contrast, those resonances that are almost purely triplet states are very broad with short, picosecond lifetimes. This is easily rationalized in terms of a state with a predominantly singlet character decaying more slowly to the triplet continuum than an (almost) purely triplet state. Visibly, the spin-orbit coupling is responsible for the predissociation decay of the Feshbach resonances, i.e., a smaller spin-orbit interaction favours longer-lasting quasi-bound states, cf. $v' = 114$ reported in Table VII.

It was shown in Ref.[78] that the widths of the resonances are very sensitive to the quality of the *ab initio* data. Since the existence of low-lying Feshbach resonances is mostly due to the spin-orbit coupling $\xi_1(R)$, between the $c^3\Pi_u$ and $A^1\Sigma_u^+$ states, we have checked how scaling this particular term by a parameter $\lambda$ ranging from 0.9 to 1.1, $\lambda \cdot \xi_1(R)$, affects the results. This is illustrated in the right-hand panel of Fig. 9. Inspection of this figure shows the width to be indeed a rather sensitive function of the coupling, and a 10% change in the coupling may result in a change of the width by a factor of two. However, since scaling within $\pm$10% does not change the order of magnitude of the lifetimes, our conclusions concerning a possible experimental observation of the Feshbach resonances in the $A^1\Sigma_u^+$, $c^3\Pi_u$, and $a^3\Sigma_u^+$ manifold remain valid.

## IV. SUMMARY AND CONCLUSIONS

We have reported a theoretical study of interatomic interactions and spectroscopy of the strontium dimer in the $A^1\Sigma_u^+$, $c^3\Pi_u$, and $a^3\Sigma_u^+$ manifold of electronic states. The spectroscopic characteristics of the potential energy curves for the nonrelativistic $A^1\Sigma_u^+$, $c^3\Pi_u$, and $a^3\Sigma_u^+$ states of $Sr_2$ and of the relativistic states of $0_u^+$ and $1_u$ symmetry deviates significantly from most of the previous *ab initio* results[15,16]. This is particularly true for the

optically active $A^1\Sigma_u^+$ state and its Hund case ($c$) analog, $(1)0_u^+$. By contrast, the present spectroscopic characteristics of the $(1)0_u^+$ state are in a very good agreement with the experimental values deduced from the high-resolution Fourier transform spectroscopic data[6]. The rovibrational energy levels corresponding to the spin-orbit coupled $(1)0_u^+$ state dissociating into $^1S_0 + {}^3P_1$ atoms lying below the avoided crossing with the $(2)0_u^+$ state dissociating into $^1S_0 + {}^1D_2$ atoms are almost unperturbed, and the corresponding energies are very close to the energies obtained in the Born-Oppenheimer approximation. The rovibrational levels of the $(1)0_u^+$ state lying above the avoided crossing with the $(2)0_u^+$ state are all heavily perturbed by the rovibrational states of the c state. These perturbations are exclusively due to the spin-orbit interaction. In all cases, the nonadiabatic effects due to the Coriolis couplings were shown to be negligible, with the exception of a few least bound levels. We have located several quasi-bound Feshbach resonances lying above the $^1S_0 + {}^3P_1$ dissociation limit. Their lifetimes suggest that they should be observable in high-resolution spectroscopic experiments.

Overall, our results reproduce (semi)quantitatively the experimental data observed thus far[6]. Our spectroscopic predictions for on-going and future experiments concerning the photoassociation of ultracold strontium atoms[26,33] and precision measurements of the time variation of the electron to proton mass ratio[27,28] are reported elsewhere[77].

## ACKNOWLEDGMENTS

We would like to thank Eberhard Tiemann, Paul Julienne, Svetlana Kotochigova and Tanya Zelevinsky for many useful discussions. Financial support from the Polish Ministry of Science and Higher Education through the project N N204 215539 and from the Deutsche Forschungsgemeinschaft through the Emmy Noether programme are gratefully acknowledged.

[1] A. Stein, H. Knöckel, and E. Tiemann, Eur. Phys. J. D **57**, 171 (2010)
[2] T. Bergeman and P. F. Liao, J. Chem. Phys. **72**, 886 (1980)
[3] G. Gerber, R. Moller, and H. Schneider, J. Chem. Phys. **81**, 1538 (1984)
[4] J. C. Miller, B. S. Ault, and L. Andrews, J. Chem. Phys. **67**, 2478 (1977)
[5] J. C. Miller and L. Andrews, J. Chem. Phys. **69**, 936 (1978)
[6] A. Stein, H. Knöckel, and E. Tiemann, Eur. Phys. J. D **64**, 227 (2011)
[7] R. O. Jones, J. Chem. Phys. **71**, 1300 (1979)
[8] G. Ortiz and P. Ballone, Phys. Rev. B **43**, 6376 (1991)
[9] J. F. Stanton, Phys. Rev. A **49**, 1698 (1994)
[10] N. A. Lima and M. J. Caldas, Phys. Rev. B **72**, 033109 (2005)
[11] J. Mitroy and M. W. J. Bromley, Phys. Rev. A **68**, 052714 (2003)
[12] S. Porsev and A. Derevianko, J. Exp. Theor. Phys. **102**, 195 (2006)
[13] J. Mitroy and J. Zhang, Mol. Phys. **108**, 1999 (2010)
[14] N. Boutassetta, A. R. Allouche, and M. Aubert-Frécon, Phys. Rev. A **53**, 3845 (1996)
[15] E. Czuchaj, M. Krosnicki, and H. Stoll, Chem. Phys. Lett. **371**, 401 (2003)
[16] S. Kotochigova, J. Chem. Phys. **128**, 024303 (2008)
[17] S. Kraft, F. Vogt, O. Appel, F. Riehle, and U. Sterr, Phys. Rev. Lett. **103**, 130401 (2009)
[18] S. Stellmer, M. K. Tey, B. Huang, R. Grimm, and F. Schreck, Phys. Rev. Lett. **103**, 200401 (2009)
[19] Y. N. M. de Escobar, P. G. Mickelson, M. Yan, B. J. DeSalvo, S. B. Nagel, and T. C. Killian, Phys. Rev. Lett. **103**, 200402 (2009)
[20] S. Stellmer, M. K. Tey, R. Grimm, and F. Schreck, Phys. Rev. A **82**, 041602 (2010)
[21] P. G. Mickelson, Y. N. Martinez de Escobar, M. Yan, B. J. DeSalvo, and T. C. Killian, Phys. Rev. A **81**, 051601 (2010)
[22] T. Fukuhara, S. Sugawa, and Y. Takahashi, Phys. Rev. A **76**, 051604 (2007)
[23] Y. Takasu, K. Maki, K. Komori, T. Takano, K. Honda, M. Kumakura, T. Yabuzaki, and Y. Takahashi, Phys. Rev. Lett. **91**, 040404 (2003)
[24] R. Ciuryło, E. Tiesinga, and P. S. Julienne, Phys. Rev. A **71**, 030701 (2005)
[25] S. Tojo, M. Kitagawa, K. Enomoto, Y. Kato, Y. Takasu, M. Kumakura, and Y. Takahashi, Phys. Rev. Lett. **96**, 153201 (2006)
[26] T. Zelevinsky, M. M. Boyd, A. D. Ludlow, T. Ido, J. Ye, R. Ciuryło, P. Naidon, and P. S. Julienne, Phys. Rev. Lett. **96**, 203201 (2006)
[27] T. Zelevinsky, S. Kotochigova, and J. Ye, Phys. Rev. Lett. **100**, 043201 (2008)
[28] S. Kotochigova, T. Zelevinsky, and J. Ye, Phys. Rev. A **79**, 012504 (2009)
[29] K. Beloy, A. W. Hauser, A. Borschevsky, V. V. Flambaum, and P. Schwerdtfeger, Phys. Rev. A **84**, 062114 (2011)
[30] D. DeMille, Phys. Rev. Lett. **88**, 067901 (2002)
[31] S. Ospelkaus, K.-K. Ni, D. Wang, M. H. G. de Miranda, B. Neyenhuis, G. Quéméner, P. S. Julienne, J. L. Bohn, D. S. Jin, and J. Ye, Science **327**, 853 (2010)
[32] Y. N. Martinez de Escobar, P. G. Mickelson, P. Pellegrini, S. B. Nagel, A. Traverso, M. Yan, R. Côté, and T. C. Killian, Phys. Rev. A **78**, 062708 (2008)
[33] T. Zelevinsky, private communication (2011)
[34] B. Bussery-Honvault, J.-M. Launay, and R. Moszynski, Phys. Rev. A **68**, 032718 (2003)
[35] B. Bussery-Honvault, J.-M. Launay, and R. Moszynski, Phys. Rev. A **72**, 012702 (2005)
[36] B. Bussery-Honvault and R. Moszynski, Mol. Phys. **104**, 2387 (2006)
[37] B. Bussery-Honvault, J.-M. Launay, T. Korona, and R. Moszynski, J. Chem. Phys. **125**, 114315 (2006)
[38] C. P. Koch and R. Moszynski, Phys. Rev. A **78**, 043417 (2008)
[39] L. Rybak, Z. Amitay, S. Amaran, R. Kosloff, M. Tomza, R. Moszynski, and C. P. Koch, Faraday Discuss. **153**, 383 (2011)
[40] L. Rybak, S. Amaran, L. Levin, M. Tomza, R. Moszynski, R. Kosloff, C. P. Koch, and Z. Amitay, Phys. Rev. Lett. **107**, 273001 (2011)
[41] M. Krych, W. Skomorowski, F. Pawłowski, R. Moszynski, and Z. Idziaszek, Phys. Rev. A **83**, 032723 (2011)
[42] M. Tomza, F. Pawłowski, M. Jeziorska, C. P. Koch, and R. Moszynski, Phys. Chem. Chem. Phys. **13**, 18893 (2011)
[43] H. Sekino and R. J. Bartlett, Int. J. Quantum Chem. **26**, 255 (1984)
[44] H. Koch and P. Jorgensen, J. Chem. Phys. **93**, 3333 (1990)
[45] H. Koch, O. Christiansen, P. Jorgensen, A. M. S. de Meras, and T. Helgaker, J. Chem. Phys. **106**, 1808 (1997)
[46] P. R. Bunker and P. Jensen, *Molecular Symmetry and Spectroscopy* (NRC Press, Ottawa, 1998)
[47] J. M. Brown and A. Carrington, *Rotational Spectroscopy of Diatomic Molecules* (Cambridge University Press, Cambridge, U.K., 2003)

[48] H. A. Bethe and E. E. Salpeter, *Quantum Mechanics of One- and Two-electron Atoms* (Academic Press, New York, 1957) p. 170

[49] K. M. Jones, P. S. Julienne, P. D. Lett, W. D. Phillips, E. Tiesinga, and C. J. Williams, Europhys. Lett. **35**, 85 (1996)

[50] W. Skomorowski and R. Moszynski, "Long-range spin-orbit interactions between like atoms and their QED retardation: application to the $Sr(^3P)+Sr(^1S)$ interaction" (in preparation)

[51] I. S. Lim, H. Stoll, and P. Schwerdtfeger, J. Chem. Phys. **124**, 034107 (2006)

[52] H. Partridge and C. W. Bauschlicher, Mol. Phys. **96**, 705 (1999)

[53] S. Boys and F. Bernardi, Mol. Phys. **19**, 553 (1970)

[54] T. Helgaker, H. J. A. Jensen, P. Jørgensen, J. Olsen, K. Ruud, H. Ågren, A. A. Auer, K. L. Bak, V. Bakken, O. Christiansen, S. Coriani, P. Dahle, E. K. Dalskov, T. Enevoldsen, B. Fernandez, C. Hättig, K. Hald, A. Halkier, H. Heiberg, H. Hettema, D. Jonsson, S. Kirpekar, R. Kobayashi, H. Koch, K. V. Mikkelsen, P. Norman, M. J. Packer, T. B. Pedersen, T. A. Ruden, A. Sanchez, T. Saue, S. P. A. Sauer, B. Schimmelpfennig, K. O. Sylvester-Hvid, P. R. Taylor, and O. Vahtras, DALTON, *an ab initio electronic structure program, Release 2.0* (2005), see http://www.kjemi.uio.no/software/dalton/dalton.html

[55] H.-J. Werner, P. J. Knowles, F. R. M. R. Lindh, M. Schütz, P. Celani, T. Korona, G. Rauhut, R. D. Amos, A. Bernhardsson, A. Berning, D. L. Cooper, M. J. O. Deegan, A. J. Dobbyn, E. G. F. Eckert, C. Hampel, G. Hetzer, A. W. Lloyd, S. J. McNicholas, W. Meyer, M. E. Mura, A. Nicklass, P. Palmieri, R. Pitzer, U. Schumann, H. Stoll, A. J. Stone, R. Tarroni, T. Thorsteinsson, M. Wang, and A. Wolf, *MOLPRO, version 2006.1, a package of ab initio programs* (2006), see http://www.molpro.net

[56] K. T. Tang and J. P. Toennies, J. Chem. Phys. **80**, 3726 (1984)

[57] W. J. Meath, J. Chem. Phys. **48**, 227 (1968)

[58] P. E. S. Wormer, F. Mulder, and A. Van der Avoird, Int. J. Quantum Chem. **11**, 959 (1977)

[59] T. Ćwiok, B. Jeziorski, W. Kołos, R. Moszynski, J. Rychlewski, and K. Szalewicz, Chem. Phys. Lett. **195**, 67 (1992)

[60] T. G. A. Heijmen, R. Moszynski, P. E. S. Wormer, and A. Van der Avoird, Mol. Phys. **89**, 81 (1996)

[61] V. Kokoouline, O. Dulieu, R. Kosloff, and F. Masnou-Seeuws, J. Chem. Phys. **110**, 9865 (1999)

[62] K. Willner, O. Dulieu, and F. Masnou-Seeuws, J. Chem. Phys. **120**, 548 (2004)

[63] S. Kallush and R. Kosloff, Chem. Phys. Lett. **433**, 221 (2006)

[64] U. V. Riss and H. D. Meyer, Journal of Physics B: Atomic, Molecular and Optical Physics **26**, 4503 (1

[65] D. E. Manolopoulos, J. Chem. Phys. **117**, 9552 (2002)

[66] T. Gonzalez-Lezana, E. J. Rackham, and D. E. Manolopoulos, J. Chem. Phys. **120**, 2247 (2004)

[67] H. S. Taylor, G. V. Nazaroff, and A. Golebiewski, J. Chem. Phys. **45**, 2872 (1966)

[68] S. G. Porsev, A. D. Ludlow, M. M. Boyd, and J. Ye, Phys. Rev. A **78**, 032508 (2008)

[69] See http://physics.nist.gov/PhysRefData for information about energy levels of strontium atom

[70] S. B. Nagel, P. G. Mickelson, A. D. Saenz, Y. N. Martinez, Y. C. Chen, T. C. Killian, P. Pellegrini, and R. Côté, Phys. Rev. Lett. **94**, 083004 (2005)

[71] I. Courtillot, A. Quessada-Vial, A. Brusch, D. Kolker, G.D. Rovera, and P. Lemonde, Eur. Phys. J. D **33**, 161 (2005)

[72] C. Redondo, M. S. Rayo, P. Ecija, D. Husain, and F. Castao, Chem. Phys. Lett. **392**, 116 (2004)

[73] B. Jeziorski and R. Moszynski, Int. J. Quantum Chem. **48**, 161 (1993)

[74] R. Moszynski, P. S. Żuchowski, and B. Jeziorski, Coll. Czech. Chem. Commun. **70**, 1109 (2005)

[75] T. Korona, M. Przybytek, and B. Jeziorski, Mol. Phys. **104**, 2303 (2006)

[76] A. Sadlej, Coll. Czech. Chem. Commun. **53**, 1995 (1988)

[77] W. Skomorowski, R. Moszynski, and C. P. Koch, Phys. Rev. A **85**, 043414 (2012)

[78] R. Moszynski, B. Jeziorski, A. van der Avoird, and P. E. S. Wormer, J. Chem. Phys. **101**, 2825 (1994)

[79] M. Yasuda, T. Kishimoto, M. Takamoto, and H. Katori, Phys. Rev. A **73**, 011403 (2006)

[80] R. Santra, K. V. Christ, and C. H. Greene, Phys. Rev. A **69**, 042510 (2004)

[81] S. G. Porsev, M. G. Kozlov, Y. G. Rakhlina, and A. Derevianko, Phys. Rev. A **64**, 012508 (2001)

[82] D. Husain and G. Roberts, Chem. Phys. **127**, 203 (1988)